

Volatilization of High Molecular Weight DNA by Pulsed Laser Ablation of Frozen Aqueous Solutions

RANDALL W. NELSON, MATTHEW J. RAINBOW, DENNIS E. LOHR, PETER WILLIAMS*

DNA has been volatilized by pulsed laser ablation of a thin film of a frozen aqueous DNA solution. The target film was irradiated in vacuum by a pulsed laser at power densities sufficient to ablate the ice matrix. The expanding ablated water vapor entrained embedded DNA molecules and expelled them into the gas phase. Ejection of DNA molecules as large as 410 kilodaltons was verified by collection of the ablation products and subsequent mass analysis by polyacrylamide gel electrophoresis with autoradiographic detection.

MASS SPECTROMETRIC ANALYSIS of massive biopolymers such as nucleic acids, proteins, and oligosaccharides requires a means of volatilizing the molecules without complete fragmentation or degradation. Slow heating of such molecules typically results in pyrolysis rather than volatilization, and so a number of desorption techniques have been developed that involve a very rapid input of energy into the target material, either by fast (mega-electron volt) or slow (kilo-electron volt) heavy-ion impact or by photon irradiation, to achieve desorption in a time that precludes complete degradation (1). In the past 8 years, much attention has been focused on the advantages derived from dissolving the sample to be volatilized in a liquid or solid matrix, which, in the case of kilo-electron volt ion impact desorption, can act to minimize ion beam damage (2), or, for pulsed laser desorption, can serve as a chromophore, efficiently coupling the radiative energy into the material to be volatilized (3-6). In the present study we have considered the role of a matrix in mediating ejection of large molecules into the gas phase and have developed a general pulsed laser desorption technique for biomolecules that we have applied specifically to the desorption of intact massive DNA molecules.

Desorption of large protein molecules after fast, heavy-ion impact has been shown to result from a rapid (subpicosecond), small-scale (~5%) expansion of the vibrationally excited molecules, which can generate kinetic energies of several electron volts by pushing away from their neighbors or a

substrate (7, 8). If massive molecules such as nucleic acids and very large proteins are to be desorbed, an extended region must coherently be excited, which can only be achieved by pulsed laser irradiation. However, for laser pulse lengths of tens of nanoseconds, the excitation rate is orders of magnitude slower than for fast-ion impact; to achieve kinetic energies sufficient to rupture the multiple hydrogen bonds binding the molecule to the substrate in an expansion process, the degree of expansion must be correspondingly greater. One process that produces a large volume change is a phase change, solid or liquid to vapor. We therefore decided that the first requirement for effective laser desorption of massive molecules would be to embed them in a solid volatile matrix, which, when ablated, produces an expanding vapor plume that can entrain the embedded molecules and expel them into the vapor phase.

The use of a volatile matrix with low boiling point and critical temperature should have several additional advantages. Most important, the critical temperature imposes an upper limit on the temperature attained before ablation occurs, and the free expansion of the ablated matrix vapor should produce a substantial degree of internal cooling of the entrained macromolecules, which will stabilize them against gas-phase dissociation. Cooling can be extremely rapid; for a laser focus of ~100 μm , substantial cooling should occur over a distance of ~1 mm above the surface, for example, in ~1 μs if gas velocities are ~10³ m/s (9). The matrix should be chosen for its solvent properties and for vacuum compatibility. We chose to study water, the natural solvent for most biomolecules; we assured vacuum compatibility by freezing the solu-

tion to liquid-nitrogen temperature. Water may also act as a chromophore, absorbing strongly at 2.9 μm where nucleic acids and proteins are largely transparent, but this property was not used in the present study. We studied the pulsed laser ablation, in vacuum, of DNA molecules from frozen aqueous solutions. DNA was chosen as a test material because large nucleic acids have not previously been volatilized by desorption techniques and sensitive autoradiographic techniques exist to detect and characterize ³²P-labeled DNA.

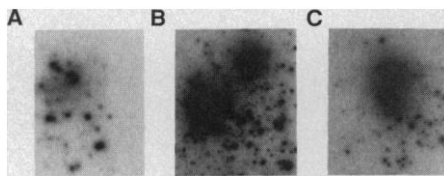
The laser target was a thin film of a frozen aqueous TE buffer (10 mM tris, 1 mM EDTA, pH 7.5) solution of an Msp I restriction enzyme digest of the *Escherichia coli* plasmid pBR322, labeled on the ends of the fragments with ³²P. The digest contained fragments of double-stranded DNA ranging in size from 9 to 622 base pairs, or ~7 to 410 kD. The solution (50 to 100 μl , 2 $\mu\text{g/ml}$) was smeared onto a copper cold finger initially cooled to -20°C, creating a thin ice film. In early work, the cold finger was acid-cleaned before each experiment and exhibited a bright metallic copper surface. After several days of applications a visible thin film of corrosion (greenish brown in color) appeared on the surface of the copper substrate. In later work the corrosion film was left on because it improved the efficiency of the ablation process, as discussed below. The cold finger was inserted into an ion-pumped vacuum system and cooled with liquid nitrogen while the system was evacuated to ~10⁻⁶ torr. The frozen films were irradiated in vacuum by 20-ns pulses from an excimer laser-pumped dye laser operating at 581 nm (wavelength of maximum laser output for the system used) at power densities ranging from ~10⁶ to ~10⁸ W/cm². We varied the laser power density at the film surface by changing the laser spot size at the target over a range of diameters between ~150 μm and ~1.5 mm, using a lens with a focal length of 150 mm. The spot sizes were estimated visually after irradiation. At 581 nm both the DNA and the water are transparent, and energy deposition occurred initially in the copper substrate. (The visible laser was the only one available to us: its use caused some complications in the ablation process, which are discussed below.) Ablated material was collected on siliconized microscope slides placed 2.0 cm away from the target. After the slides had been removed from the vacuum system, direct-contact autoradiograms of the collector slides were obtained.

Two distinct angular distributions were typically observed on the collector slide, indicating the existence of two distinct transport processes. When visibly thick layers of the frozen films were irradiated, the

Department of Chemistry, Arizona State University, Tempe, AZ 85287.

*To whom correspondence should be addressed.

Fig. 1. Direct-contact autoradiograms (A–C) of collector slides showing angular distributions. Spallation can be recognized as randomly distributed discrete spots, whereas ablation is recognized by the diffuse, highly forward-peaked angular distributions indicative of a vapor-phase expansion. Material was selectively extracted from the collector slide with TE buffer. Each slide was placed over its corresponding autoradiogram, so that the positions of the various deposits were known. Four separate 10- μ l droplets of TE were placed successively onto an area of interest, moved within its confines to dissolve the deposit, and then combined for loading into the gel. By keeping the volume of each extraction small, we could control the area from which material was recovered.



collected deposits consisted almost entirely of randomly dispersed small spots (millimeter to submillimeter diameter). We ascribe these spots to spallation of macroscopic ice fragments driven by the formation of vapor bubbles beneath the films. When thin regions of the ice films (≤ 10 μ m thick, estimated from the pressure pulses on the ion pump power supply) were irradiated, some spallation spots were still observed, but most of the radioactivity collected was concentrated in diffuse but strongly forward-peaked deposits (Fig. 1, A through C), as expected for the free expansion of the vapor

from the laser-ablated areas (10).

Subsequent polyacrylamide gel electrophoresis (PAGE) indicated that the material extracted from the spallation deposits had size distributions (Fig. 2A) identical to those of the starting digest (Fig. 2E), indicating that DNA had been transported across the vacuum gap intact (encapsulated in the ice fragments), as would be expected. PAGE results for material selectively extracted from the centers of the diffuse ablation deposits were qualitatively different (Fig. 2, B through D). The size distributions showed that the DNA transported by the ablation process had been fragmented to varying degrees; superimposed on the continuous fragment distributions were bands corresponding to DNA with the same mass distribution as that of the starting material.

The degree of fragmentation depended on the laser power density and the nature of the substrate surface. The extensive fragmentation observed in Fig. 2B was obtained by using a laser power density of $\sim 4 \times 10^6$ W/cm² on an acid-cleaned copper substrate; little or no corrosion was present. When the laser power density was increased to $\sim 2 \times 10^8$ W/cm², till with a clean copper substrate, well-defined bands (corresponding to intact digest molecules) appeared superimposed on the fragment continuum, showing that more of the analyte molecules survived intact (Fig. 2C). The size distribution in Fig. 2D was obtained from ablated material collected after a thin frozen film on a corroded copper substrate had been irradiated at a laser power density of $\sim 2 \times 10^8$ W/cm². Although fragmentation was still evident, the size distribution was dominated by bands representing intact analyte molecules, even at the higher mass range (309 to 622 bp). These effects appear to be related to the rate of heating of the ice target. Increasing the power input, by raising the laser power density, by increasing the absorptivity of the substrate, or by any combination of these effects, increases the rate of transfer of heat from the substrate to the ice film. Increasing the power input rate by using shorter laser pulses reduces the extent of fragmentation of laser-ablated small molecules (11).

Results similar to those shown in Figs. 1 and 2 were obtained in a series of replicate experiments at laser power densities between $\sim 1 \times 10^6$ and $\sim 2 \times 10^8$ W/cm² on both acid-cleaned and corroded copper substrates. Laser irradiation of thin films at power densities less than $\sim 4 \times 10^6$ W/cm² produced similar, highly forward-peaked angular distributions, indicating that comparable amounts of radioactivity had been transported to the collector slide by ablation; however, electrophoresis results indicated that these deposits contained no DNA within the mass range of the gel (lower limit, ~ 20 kD), suggesting that multiple fragmentation had occurred. Control experiments, without laser irradiation, with the sample cold or slowly warmed to room temperature, confirmed that no material transfer occurred as a result of the radioactivity of the target or as a result of any spontaneous processes such as spallation of ice crystals. Irradiation, at laser power densities of $\sim 2 \times 10^8$ W/cm², of a thin film that had been allowed to dry transported radioactivity to the collector slide, but no DNA fragments were seen within the mass range of the gel used.

Pulsed laser ablation of frozen aqueous solutions appears to be a general volatilization technique for biomolecular mass spectrometry. Given the production of vapor-phase molecules, mass spectrometry requires, in addition, ionization, mass analysis, and detection steps. Molecules ablated from a solution of a non-isoelectric pH may intrinsically be charged; if not, ionization, by electron impact, multiphoton absorption, or chemical ionization is routine. Mass analysis by time-of-flight techniques has no upper mass limit. Detection of massive ions has been considered a problem, but recently detection of protein molecules up to 200 kD has been shown by Karas *et al.* to be possible with the use of a conventional ion-electron multiplier operated at high ion-impact energy (12). The varying degree of fragmentation evident in the DNA mass distributions appears to result from the different rates of energy input into the matrix and therefore may be controllably induced by varying the laser power density. In that small oligonucleotides undergo thermal fragmentation preferentially at the phosphodiester linkage (13), direct acquisition of sequence information in the mass spectrometer may be possible.

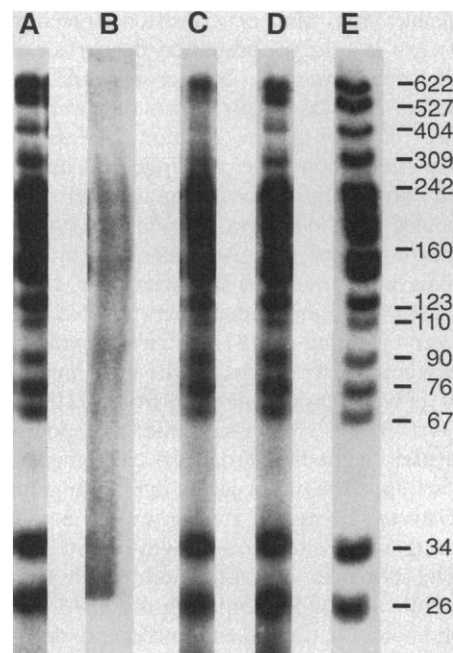


Fig. 2. Autoradiograms indicating the mass distributions of ³²P end-labeled pBR322 Msp I DNA digest obtained by use of 6% polyacrylamide gel electrophoresis. Molecular weights are in base pair units (1 bp, ~ 660 daltons). (A) Spallation: material collected from spallation deposits in Fig. 1C. (Material extracted from the areas containing spallation deposits in Fig. 1, A and B, gave size distributions identical to this track.) (B–D) Analysis of ablation products: (B) laser power density, $\sim 4 \times 10^6$ W/cm²; clean copper substrate (ablation deposit, Fig. 1A); (C) laser power density, $\sim 2 \times 10^8$ W/cm²; clean copper substrate (two ablation deposits, Fig. 1B); (D) laser power density, $\sim 2 \times 10^8$ W/cm²; corroded copper substrate (ablation deposit, Fig. 1C). (E) Starting digest, no laser irradiation.

REFERENCES AND NOTES

- See, for example, *Ion Formation from Organic Solids*, vol. III, A. Benninghoven, Ed. (Springer-Verlag, Berlin, 1985).
- D. J. Surman and J. C. Vickerman, *J. Chem. Res. (S)*, 170 (1981).
- M. Karas, D. Bachman, F. Hillenkamp, *Anal. Chem.* 57, 2935 (1985).

4. K. Tanaka *et al.*, *Rapid Commun. Mass Spectrom.* **2**, 151 (1988).
5. M. Karas, D. Bachman, U. Bahr, F. Hillenkamp, *Int. J. Mass Spectrom. Ion Processes* **78**, 53 (1987).
6. M. Karas and F. Hillenkamp, *Anal. Chem.* **60**, 2299 (1988).
7. P. Williams and B. U. R. Sundqvist, *Phys. Rev. Lett.* **58**, 1031 (1987).
8. D. Fenyo *et al.*, *J. Phys. (Paris) C 2*, 33 (1989).
9. J. B. Fenn, in *Applied Atomic Collision Physics*, H. S. W. Massey, E. W. McDaniel, B. Bederson, Eds. (Academic Press, New York, 1982), vol. 5, pp. 349–378.
10. R. Kelly and R. W. Dreyfus, *Nucl. Instrum. Methods Phys. Res. B* **32**, 341 (1988).
11. L. Q. Huang, R. J. Conzemius, G. A. Junk, R. S. Houk, *Anal. Chem.* **60**, 1490 (1988).
12. M. Karas, A. Ingendoh, U. Bahr, F. Hillenkamp, *Biomed. Environ. Mass Spectrom.* **18**, 841 (1989).
13. J. L. Wiebers, in *High Performance Mass Spectrometry: Chemical Applications*, M. L. Gross, Ed. (ACS Symposium Series 70, American Chemical Society, Washington, DC, 1978), p. 248.
14. The work of D.E.L. was supported under NIH grants RCDA CA 00911 and GM 37788. R.W.N. was partly supported by personal funds (P.W.). We are deeply indebted to J. D. Gust for allowing us free access to the laser system.

21 July 1989; accepted 18 October 1989

Growth of Greenland Ice Sheet: Measurement

H. JAY ZWALLY, ANITA C. BRENNER, JUDY A. MAJOR,
ROBERT A. BINDSCHADLER, JAMES G. MARSH

Measurements of ice-sheet elevation change by satellite altimetry show that the Greenland surface elevation south of 72° north latitude is increasing. The vertical velocity of the surface is 0.20 ± 0.06 meters per year from measured changes in surface elevations at 5906 intersections between Geosat paths in 1985 and Seasat in 1978, and 0.28 ± 0.02 meters per year from 256,694 intersections of Geosat paths during a 548-day period of 1985 to 1986.

DETERMINATION OF THE BALANCE between mass input and outflow of the polar ice sheets is needed for understanding of the ice-sheet response to climate change and the contributions to sea-level rise or fall. Measurement of elevation change by satellite altimetry offers a method of determining changes in ice volume and therefore mass balance (1). The 3-year operation of GEOS-3 radar altimeter from April 1975 to June 1978 (2), followed by the 3-month operation of the Seasat radar altimeter from July to September 1978, provided a time series of ice elevations, but the precision and spatial coverage of GEOS-3 was limited. The U.S. Navy Geosat radar altimeter (3), which was launched in March 1985, has provided a large number of recent repetitive measurements. We have determined changes in ice-surface elevations using data from GEOS-3, Seasat, and the first 18 months of Geosat. The estimated change in ice volume and its significance is discussed in a companion paper (4).

Changes in surface elevation were determined where successive sub-satellite paths intersect (Fig. 1). The measured elevation difference at a crossover point is $dH =$

$H_2 - H_1 + E$, where H_2 and H_1 are the surface elevations during successive orbits at times t_2 and t_1 , respectively, and E is the random measurement error from a distribution with a SD. The error for each elevation measurement is $E/\sqrt{2}$, which includes errors in the altimeter-range measurement and in determination of the vertical position of the orbit. The magnitude of E is determined from analysis for which $(H_2 - H_1)$ are small. Although E is usually larger than actual elevation changes, average changes can be obtained over areas of the ice sheet for time periods in which there are a sufficiently large number of measurements.

The range measured (Fig. 1) is to the average surface elevation in the "pulse-limited" footprint [maximum circular area from which radar reflection is simultaneously received by the altimeter (2, 5)]. The minimum pulse-limited footprint is 3.6 km in diameter for the GEOS-3 altimeter and 1.6 km for both the Seasat and Geosat altimeters, over smooth surfaces and larger over

rough surfaces. Ranges are obtained at 0.66-km intervals along the satellite tracks; therefore, successive footprints overlap by 40% or more. Surface elevations at the crossover point are obtained by interpolation. Determination of the absolute surface elevation at satellite nadir would require correction for the slope-induced offset of the pulse-limited footprint from nadir (6), which is caused by the tendency of the pulse-limited footprint to be located at the closest surface lying within the larger "beam-limited" footprint, which is ten times the size of the pulse-limited footprint (5). However, for the purpose of studying elevation changes, correction for slope-induced errors is not necessary because the pulse-limited footprint is usually located at the same place on the surface during successive transits.

We corrected surface elevations for variations in the effective atmospheric path length, earth tides, and lags in the automatic radar-pulse tracking circuitry of the altimeter (3, 4). For GEOS-3 and Seasat, residual errors in the radial position of the satellite with respect to the center of the earth are reduced by reference of the orbital positions to a common ocean surface derived from the Seasat and GEOS-3 altimeter data. After orbit adjustment, the SD of the elevation differences is 4.7 m for GEOS-3–GEOS-3 crossovers and 1.0 m for Seasat–Seasat crossovers. The standard errors for single measurements are 3.3 m for GEOS-3 and 0.70 m for Seasat. The calculated SD for GEOS-3–Seasat differences is 3.4 m. Precise orbit information over ice-covered areas is included with the Geosat data (7). The SD of the elevation differences at 16,250 Geosat–Geosat crossovers for which the time difference between measurements is <15 days is 1.49 m. The Geosat single-measurement error is therefore 1.05 m. In these analyses, crossover differences greater than 10 m were discarded (15 m for GEOS-3) (8). The relative SD for Geosat–Seasat differences is therefore 1.26 m. The remaining errors are mainly a combination of altimeter measurement error over irregular surfaces and residual orbit errors.

Two methods were used to obtain the rate of change of surface elevation from a set of

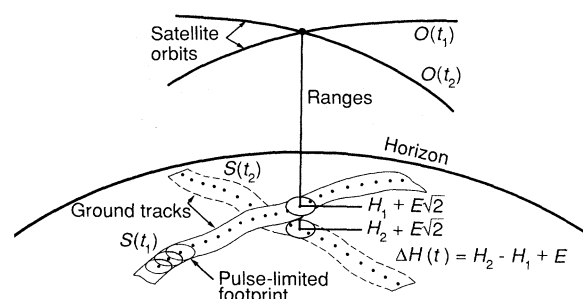


Fig. 1. Crossover method for measuring changes in surface elevation, $S(t)$, from radar-altimeter measured elevations, $H(t)$, on successive orbital paths (O) of the satellite. Horizontal location of the crossover point is determined within a few meters. The relative error, E , for measurement of elevation change, dH , at a single crossover is about 1.4 m.

H. J. Zwally and R. A. Bindschadler, Oceans and Ice Branch, Code 671, National Aeronautics and Space Administration (NASA), Goddard Space Flight Center, Greenbelt, MD 20771.
A. C. Brenner and J. A. Major, ST Systems Corporation, 4400 Forbes Way, Lanham, MD 20706.
J. G. Marsh, Space Geodesy Branch, Code 626, NASA, Goddard Space Flight Center, Greenbelt, MD 20771.